The $5f^2 \rightarrow 5f^1 6d^1$ absorption spectrum of Cs_2GeF_6 : U^{4+} crystals: A quantum chemical and experimental study

Belén Ordejón
Departamento de Química, C-XIV, Universidad Autónoma de Madrid, 28049 Madrid, Spain

Miroslaw Karbowiak
Faculty of Chemistry, University of Wroclaw, ul. F. Joliot-Curie 14, 50-383, Wroclaw, Poland

Luis Seijo and Zoila Barandiarán[a]
Departamento de Química, C-XIV, Universidad Autónoma de Madrid, 28049 Madrid, Spain and Instituto Universitario de Ciencia de Materiales Nicolás Cabrera, Universidad Autónoma de Madrid, 28049 Madrid, Spain

Single crystals of U^{4+}-doped Cs_2GeF_6 with 1% U^{4+} concentration have been obtained by the modified Bridgman-Stockbarger method in spite of the large difference in ionic radii between Ge^{4+} and U^{4+} in octahedral coordination. Their UV absorption spectrum has been recorded at 7 K, between 190 and 350 nm; it consists of a first broad and intense band peaking at about 38 000 cm^{-1} followed by a number of broad bands of lower intensity from 39 000 to 45 000 cm^{-1}. None of the bands observed shows appreciable fine vibronic structure, so that the energies of experimental electronic origins cannot be deduced and the assignment of the experimental spectrum using empirical methods based on crystal field theory cannot be attempted. Alternatively, the profile of the absorption spectrum has been obtained theoretically using the U–F bond lengths and totally symmetric vibrational frequencies of the ground $5f^2 - 1A_{1g}$ and $5f^1 6d(t_{2g})^1 - iT_{1u}$ excited states, their energy differences, and their corresponding electric dipole transition moments calculated using the relativistic *ab initio* model potential embedded cluster method. The calculations suggest that the observed bands are associated with the lowest five $5f^2 - 1A_{1g} \rightarrow 5f^1 6d(t_{2g})^1 - iT_{1u}$ ($i = 1-5$) dipole allowed electronic origins and their vibrational progressions. In particular, the first broad and intense band peaking at about 38 000 cm^{-1} can be safely assigned to the 0-0 and 0-1 members of the a_{1g} progression of the $5f^2 - 1A_{1g} \rightarrow 5f^1 6d(t_{2g})^1 - 1T_{1u}$ electronic origin. The electronic structure of all the states with main configurational character $5f^1 6d(t_{2g})^1$ has been calculated as well. The results show that the lowest crystal level of this manifold is $5f^1 6d(t_{2g})^1 - 1E_u$ and lies about 6200 cm^{-1} above the $5f^2$ level closest in energy, which amounts to some 11 vibrational quanta. This large energy gap could result in low nonradiative decay and efficient UV emission, which suggest the interest of investigating further this new material as a potential UV solid state laser. © *2006 American Institute of Physics.* [DOI: 10.1063/1.2336427]

I. INTRODUCTION

Wide band gap insulators, in particular, fluoride hosts, are a common choice for doping lanthanide and actinide ions as activators because their large transparency window allows for the study of high energy electronic states in the UV or VUV, such as the $4f^{n-1}5d^1$ or $5f^{n-1}6d^1$ levels. Many interesting optical properties of the activated crystals depend on these levels and on their relative energies with respect to the $4f^n$ or $5f^n$ manifolds. Recently, the potentiality of U^{4+} defects in fluoride hosts as either phosphors based on quantum cutting in the visible range or as tunable UV solid state lasers has been pointed out and investigated.[1–5] The host crystals used in these works ($YLiF_4$ and YF_3) accommodate the U^{4+} ions in low symmetry Y^{3+} sites, creating charged defects in high coordination (8 and 9, respectively).[1–5] The need for

charge compensation results in the occurrence of several local defects whose structure and distribution across the crystal are difficult to determine and whose spectroscopic properties sum up leading to complex spectra. In this context, the interest of studying U^{4+} neutral defects in highly symmetric (in particular, centrosymmetric) fluoride hosts was pointed out as an alternative to the complications associated with multisites in low symmetry,[6] and a theoretical study of the $5f^2$ manifold of U^{4+} defects in cubic Cs_2GeF_6 crystals was done[6] using the relativistic *ab initio* model potential (AIMP) embedded cluster method.[7,8] In the Cs_2GeF_6 crystal, U^{4+} ions substitute for Ge^{4+} host ions creating neutral, octahedral $(UF_6)^{2-}$ defects. The U–F bond lengths of all $5f^2$ states were calculated and found to be quite constant, so that the average bond length over the whole manifold and the standard deviation of the individual values relative to the average were found to be 2.174 ± 0.005 Å.[6] When compared with the Ge–F bond length in the perfect host [1.80 Å (Ref. 9)] this result showed a large outward distortion by some 0.37 Å caused by

---
[a]Author to whom correspondence should be addressed. Electronic mail: zoila.barandiaran@uam.es

the much larger U^{4+} impurity [the estimated ionic radius of U^{4+} is larger than that of Ge^{4+} in sixfold coordination by some 0.44 Å (Refs. [10] and [11])]. Whether such a large local distortion could result in difficulties in the growth of $Cs_2GeF_6:U^{4+}$ single crystals was not addressed in Ref. [6], leaving this question open to experimental confirmation. Together with their local structure, the energies of the $5f^2$ levels were obtained and analyzed, which allowed to suggest which are the possible $5f^2$ luminescent levels. In particular, $Cs_2GeF_6:U^{4+}$ was ruled out as a phosphor material based on cascade emission initiating in the $5f^2$ crystal level emparented with the U^{4+} $^1S_0$ state.[6] This conclusion shifted the interest towards a detailed study of the electronic structure of the $5f^16d^1$ manifold, whose lowest levels could be responsible for intense UV absorption and laser emission. Taking all this into account, we decided to conduct an experimental and theoretical work in order to investigate (i) whether U^{4+}-doped Cs_2GeF_6 single crystals can be grown in spite of the large difference in ionic sizes and (ii) whether intense UV absorption could be experimentally detected and theoretically interpreted and assigned, which would encourage further research of this new material as a potential UV solid state laser.

As we show in this work, U^{4+}-doped Cs_2GeF_6 single crystals with 1% U^{4+} concentration were obtained by the Bridgman-Stockbarger method, in spite of the large local distortion due to U^{4+}. Their absorption spectrum was measured at 7 K, between 190 and 350 nm. It consists of a first broad and intense band peaking at about 38 000 cm^{-1} followed by a number of broad bands of much lower intensity from 39 000 to 45 000 cm^{-1}. None of the bands observed shows appreciable fine vibronic structure, so that the energies of experimental electronic origins cannot be deduced and the assignment of the experimental spectrum using empirical methods based on crystal field theory cannot be attempted. Alternatively, the relativistic AIMP embedded cluster method has been used in this work to calculate the electronic structure of the $5f^16d(t_{2g})^1$ manifold, which leads to the energies of the $5f^2 \rightarrow 5f^16d(t_{2g})^1$ electronic origins, the oscillator strengths of the electric dipole allowed $5f^2-1A_{1g} \rightarrow 5f^16d(t_{2g})^1-iT_{1u}$ $(i=1,11)$ transitions, and the band profile of the absorption spectrum, which, in comparison with the experimental absorption band profile, has enabled the assignment of the observed UV absorption spectrum as due to intense $5f^2 \rightarrow 5f^16d(t_{2g})^1$ electric dipole allowed transitions, this pointing out the $Cs_2GeF_6:U^{4+}$ crystals as candidates of UV solid state laser materials. The agreement between the theoretical and experimental absorption spectra encourages the use of the AIMP embedded cluster method as a predictive tool that can be applied to materials that have not been synthesized to explore the potential interest of their electronic structure and experimental study. The results presented in this work also suggest that doping lanthanide or actinide impurities in highly symmetric fluorides (such as Cs_2GeF_6, cubic fluoroelpasolites, etc.) should be considered even when the difference in ionic radii of the impurity and the substituted ion is large.

II. EXPERIMENTAL METHODS

The starting materials for the synthesis of $Cs_2GeF_6:U^{4+}$ crystals were Cs_2CO_3, $GeCl_4$, and UF_4. 15.0 g of Cs_2CO_3 was dissolved in small amount of water in a 100 ml Teflon beaker over the hot plate and concentrated HCl was added dropwise until the evolution of carbon dioxide ceased. Then 5 g of $GeCl_4$ was added and the solution volume was adjusted with water to 25 ml. Afterwards, 25 ml of HF (40%) was added to the above solution leading to immediate precipitation of the product Cs_2GeF_6 as a dense crystalline powder, which was isolated by filtration. The obtained powder was checked for phase purity by x-ray powder diffractometry. UF_4 was precipitated in anhydrous methanol by dropping an excess of NH_4F solution to that of uranium tetrachloride. The Cs_2GeF_6 and UF_4 powders were dried by heating under high dynamic vacuum and the former compound was additionally purified prior to the crystal growth by passing through the Bridgman furnace.

The well grounded mixture of Cs_2GeF_6 and UF_4 in 100:1 molar ratio was put in a glassy carbon crucible, which was next placed in a quartz ampoule, sealed under reduced pressure (0.5 atm) of argon, and passed through the vertical Bridgman furnace. The temperature of the melting zone was set at 820 °C and the crucible was lowered at a rate of 2 mm/h. The sample for absorption spectrum measurements was cleaved from the as grown boule crystal and was of good optical quality.

Absorption spectra have been recorded on Cary 500 Scan UV-Vis-NIR spectrophotometer in 190–350 nm range. For low temperature measurements the crystal was mounted in a helium Oxford Instruments optical cryostat and cooled to 7 K.

III. THEORETICAL METHODS

In what follows, the details of the calculations of the potential energy surfaces of the $5f^16d^1$ excited states of the $(UF_6)^{2-}$ defect cluster embedded in the Cs_2GeF_6 crystal are given. They have been done using the relativistic AIMP embedded cluster method.[7,8] According to this method, the following group wave functions are calculated in the $Cs_2GeF_6:U^{4+}$ crystal: $\Phi^{(UF_6)^{2-}}(i\Gamma)$, which are the defect cluster wave functions, belonging to irrep Γ of the octahedral double group, and Φ^S $(S=Cs^+, Ge^{4+}, F^-)$, which are wave functions of the lattice ions external to the cluster. They are calculated at very different levels of methodology, in agreement with the assumption that the optical properties of interest are primarily determined by the $(UF_6)^{2-}$ electronic structure under the influence of the crystalline environment. Whereas the $\Phi^{(UF_6)^{2-}}(i\Gamma)$ cluster wave functions and energies are calculated using a relativistic embedded cluster Hamiltonian at the highest methodological level possible, using multireference multiconfigurational methods of quantum chemistry (see below), the external ion wave functions Φ^S are calculated at the simplest Hartree-Fock (HF) level, in a preparatory, iterative self-consistent embedded ions (SCEI) calculation in $Cs_2GeF_6:S$, with only one purpose: to provide the embedding potentials acting on the defect cluster $(UF_6)^{2-}$. In each cycle of the SCEI calculation, the Φ^S HF

embedded ion wave functions are used to produce one-electron, nonparametric embedding potentials according to the AIMP recipes;[7] the procedure ends when the Φ^S wave functions and the embedding AIMP they produce are self-consistent. Then, these embedding potentials become part of the Hamiltonian used to calculate the $\Phi^{(UF_6)^{2-}}(i\Gamma)$ embedded cluster wave functions and energies. The embedding AIMPs consist of long-range Coulomb operators (point charge or Madelung potential) and short-range Coulomb, exchange, and projection operators which represent the physical interactions between the cluster wave functions and the frozen HF external Φ^S, including antisymmetry between the $\Phi^{(UF_6)^{2-}}(i\Gamma)$ and Φ^S electronic group functions.[7,8] Once the AIMP embedding is obtained and added to the cluster Hamiltonian, the calculations formally proceed as in isolated molecules, using standard molecular quantum chemistry methods and codes. At this point, the focus is on the proper representation of electron correlation and relativistic effects within the $(UF_6)^{2-}$ electronic group function. For the latter purpose, the AIMP method is also used as a relativistic, two-component effective core potential method,[8,12] which reduces the number of electrons that are explicitly treated in the $(UF_6)^{2-}$ group and facilitates the incorporation of relativistic effects, up to spin-orbit coupling, and electron correlation through an approximate, but efficient decoupling technique based on the use of spin-free-state-shifting operators.[13]

The embedding potentials that represent the quantum mechanical effects of the Cs$_2$GeF$_6$ host onto the $(UF_6)^{2-}$ cluster in the Cs$_2$GeF$_6$:$(UF_6)^{2-}$ calculations presented here were obtained elsewhere[14] and were used in the calculations of the $5f^2$ manifold of Cs$_2$GeF$_6$:U^{4+}.[6]

Within the $(UF_6)^{2-}$ cluster, relativistic core AIMPs were used to represent the $[Xe, 4f]$ core of U (Ref. 15) and the [He] cores of F (Ref. 16). The corresponding U valence basis set $(14s10p12d9f)$,[17] supplemented with three g-type functions that give maximum radial overlap with the $5f$ atomic orbital, was used contracted as $[6s5p6d4f1g]$. In the case of F, the valence basis set used $(5s6p1d)$ $[3s4p1d]$ (Ref. 16) includes one p-type diffuse function for anions[18] and one d-type polarization function.[19] Electron correlation and spin-orbit coupling were combined together as follows. In a first, spin-orbit free step, state-average complete active space self-consistent field[20] (SA-CASSCF) calculations were done using the relativistic Wood-Boring AIMP (Ref. 12) embedded cluster Hamiltonian omitting the spin-orbit operators [cf. Eq. (1) in Ref. 21]. The active space results from distributing the two open-shell electrons in 13 active molecular orbitals with main character U $5f$, $6d$, $7s$; it will be referred to as CASSCF$(5f,6d,7s)$.[21] The state average extends to all $5f^16d^1$ and $5f^17s^1$ electronic states of each symmetry block (the calculations were done using D_{2h} symmetry). These calculations account for scalar relativistic effects and nondynamic electron correlation within the $5f^16d^1$ manifold. Dynamic electron correlation was taken into account in subsequent multistate second-order perturbation theory[22–25] (MS-CASPT2) calculations, where all 68 valence electrons occupying the cluster molecular orbitals of main character F $2s$, $2p$, and U $5d$, $6s$, $6p$, $5f$, and $6d$ were correlated; these calculations will be referred to as MS-CASPT2(F48, U20).

In a second, spin-dependent step, we performed double-group spin-orbit configuration interaction (CI) calculations using the whole Wood-Boring AIMP Hamiltonian.[12,21] The shifting operator included in this Hamiltonian, the so-called spin-free-state-shifting (sfss) operator,[13] transports the dynamic electron correlation effects retrieved at the spin-orbit-free MS-CASPT2(F48, U20) level onto the smaller configurational space used in the spin-orbit CI calculations, which includes the CAS$(5f,6d,7s)$ configurations plus all single excitations from the active to the virtual molecular orbitals in order to account for orbital relaxation due to spin orbit.[26] For these calculations the bases described above were truncated to U $[6s5p6d4f]$ and F $[3s4p]$.

A study of the $5f^16d^1$ excited states of U^{4+} free ion has been done to find out the errors associated with the approximations included in the methods we have just described at the atomic level, by comparing the calculated and experimental $5f^2 \rightarrow 5f^16d^1$ U^{4+} atomic spectra.[27] The atomic errors can be associated with the use of the Wood-Boring spin-orbit approximation and with the fact that the valence basis set and the electron correlation treatment are not complete, but limited as described above. The study shows that the one-electron Wood-Boring spin-orbit operator of U overestimates the atomic spin-orbit splittings by some 10%, like in other similar cases.[6,28] It also shows that the ^3F_u, ^3G_u, ^3P_u, and ^1D_u terms of U^{4+} are calculated some 1000, 1400, 700, and 800 cm^{-1} too low, respectively, the rest of SL states being also low by less than 500 cm^{-1}, at the MS-CASPT2(U20) level described above.[27] Previous works on the $5f^2$ manifold of U^{4+}-doped Cs$_2$ZrCl$_6$ (Ref. 28) and Cs$_2$GeF$_6$ (Ref. 6) crystals have shown that these atomic errors can be expected to propagate to the embedded cluster calculations and that it is convenient to use the parameters available in the Wood-Boring spin-orbit operator and in the spin-free-state-shifting operators to correct for these atomic contributions. In consequence, the spin-orbit operator of U [for details of this operator, see Refs. 8, 12, and 28, Eq. (3)],

$$\hat{h}^I_{SO}(i) = \lambda^I \sum_{n\ell \in \text{valence}} V^{I,MP}_{SO,n\ell}(r_i) \hat{O}^I_\ell \hat{l} \hat{s} \hat{O}^I_\ell, \tag{1}$$

(with $I=U$) was scaled by a factor of $\lambda^U=0.9$ in the embedded cluster calculations. Similarly, the $\delta(iS\Gamma)$ parameters of the spin-free-state-shifting operator for the $iS\Gamma$ cluster states [see details of this operator, including the definition of the $\delta(iS\Gamma)$ parameters, in Ref. 28, Eqs. (1) and (2), or in Ref. 6] have been substituted by $\delta'(iS\Gamma)$ values resulting from the addition of a term depending on the empirical atomic corrections associated with the jSL free ion terms, $\delta_{corr}(jSL)$, to the original $\delta(iS\Gamma)$ values, as follows:

$$\delta'(iS\Gamma) = \delta(iS\Gamma) + \sum_{jSL} w(jSL, iS\Gamma)\delta_{corr}(jSL). \tag{2}$$

Due to the fact that the mixture of free ion states is very large in Cs$_2$GeF$_6$, we estimate the correspondence between free ion jSL and embedded cluster $iS\Gamma$ terms and, therefore, the weights to be associated with each empirical atomic correction in Eq. (2), $w(jSL, iS\Gamma)$, taking into account the results of the following approximate projection of the embedded clus-

TABLE I. Analysis of spin-orbit-free $5f^1 6d^1$ embedded cluster wave functions, $\Phi^{(\mathrm{UF}_6)^{2-}}(iS\Gamma)$, in terms of $5f^1 6d^1$ free ion terms, $\Phi^{\mathrm{U}^{4+}}(jSL)$. The tabulated values correspond to $w(jSL,iS\Gamma)$ in Eq. (4). See text for details.

Free ion jSL terms	Embedded cluster $iS\Gamma$ terms[a]									
	$1\,^3T_{1u}$	$1\,^3T_{2u}$	$1\,^3A_{1u}$	$2\,^3T_{1u}$	$1\,^3E_u$	$1\,^3A_{2u}$	$2\,^3E_u$	$3\,^3T_{1u}$	$2\,^3T_{2u}$	$\delta_{\mathrm{corr}}(jSL)$
^3F_u	0.25	0.47				0.70		0.02	0.05	+1000
^3H_u	0.49	0.20		0.19	0.09		0.01	0.39	0.27	
^3G_u	0.06	0.14	0.75	0.36	0.39		0.32	0.21	0.05	+1400
^3D_u					0.27		0.38		0.40	+500
^3P_u	0.03			0.26				0.15		+700
Residue	0.17	0.19	0.25	0.19	0.25	0.30	0.29	0.23	0.23	
	$1\,^1A_{1u}$	$1\,^1T_{1u}$	$1\,^1E_u$	$1\,^1T_{2u}$	$2\,^1T_{1u}$	$2\,^1E_u$	$2\,^1T_{2u}$	$1\,^1A_{2u}$	$3\,^1T_{1u}$	$\delta_{\mathrm{corr}}(jSL)$
^1G_u	0.82	0.55	0.39	0.22	0.08	0.22	0.01		0.06	+200
^1D_u			0.33	0.01		0.07	0.49			+800
^1F_u		0.15		0.51	0.20			0.77		+300
^1H_u		0.02	0.05	0.06	0.51	0.52	0.26		0.35	
^1P_u		0.10			0.01				0.37	
Residue	0.18	0.18	0.23	0.20	0.20	0.19	0.24	0.23	0.22	

[a]The embedded cluster wave functions correspond to calculations at 2.17 Å U–F distance.

ter $5f^1 6d^1$ wave functions, $\Phi^{(\mathrm{UF}_6)^{2-}}(iSM_S\Gamma\gamma)$, on the $5f^1 6d^1$ free ion space, $\{\Phi^{\mathrm{U}^{4+}}(jSM_SLM_L)\}$:

$$\Phi_{\mathrm{os}}^{(\mathrm{UF}_6)^{2-}}(iSM_S\Gamma\gamma)$$
$$= \sum_{jLM_L} |\Phi_{\mathrm{os}}^{\mathrm{U}^{4+}}(jSM_SLM_L)\rangle$$
$$\times \langle\Phi_{\mathrm{os}}^{\mathrm{U}^{4+}}(jSM_SLM_L)|\Phi_{\mathrm{os}}^{(\mathrm{UF}_6)^{2-}}(iSM_S\Gamma\gamma)\rangle + \text{residue}. \quad (3)$$

In this way, the weights of the empirical atomic corrections can be estimated as

$$w(jSL,iS\Gamma) = \sum_{M_L} \langle\Phi_{\mathrm{os}}^{\mathrm{U}^{4+}}(jSM_SLM_L)|\Phi_{\mathrm{os}}^{(\mathrm{UF}_6)^{2-}}(iSM_S\Gamma\gamma)\rangle^2. \quad (4)$$

As indicated with the subscript os, the projection and, therefore, the overlaps in Eqs. (3) and (4) are calculated integrating only the open-shell parts of the SA-CASSCF wave functions $\Phi^{\mathrm{U}^{4+}}(jSM_SLM_L)$ and $\Phi^{(\mathrm{UF}_6)^{2-}}(iSM_S\Gamma\gamma)$, which have the same number of electrons; for this purpose, the same molecular basis set (described above) has been used for the free ion and for the embedded cluster wave functions, and the cluster wave functions used are those calculated at 2.17 Å U–F internuclear distance. The values of the empirical atomic corrections $\delta_{\mathrm{corr}}(jSL)$ and of the weights $w(jSL,iS\Gamma)$ needed to calculate the second term of Eq. (2) appear in Table I. The latter show the considerable mixture of free ion jSL terms in the cluster $iS\Gamma$ wave functions.

The spin-orbit-free calculations were done using the MOLCAS program system;[29] a modified version of the COLUMBUS package[30] was used for the spin-orbit CI part. The electric dipole transition moments and oscillator strengths were calculated from the spin-orbit wave functions using the program TRANSO, which is a program related to the EPCISO package.[31] All AIMP data (for embedding and for frozen cores) and valence basis sets can be found in Ref. 32.

IV. RESULTS AND DISCUSSION

A. Electronic structure of the $5f^1 6d(t_{2g})^1$ manifold

Like in other similar cases, where the point symmetry at the impurity site is octahedral, the results of the calculations show that the $5f^{n-1}6d^1$ manifold of $Cs_2GeF_6:U^{4+}$ is splitted into two sets of states that can be labeled according to their dominant spatial configuration as $5f^{n-1}6d(t_{2g})^1$ and $5f^{n-1}6d(e_g)^1$. In addition, a new manifold of states with dominant $5f^1 7s^1$ configuration appears in $Cs_2GeF_6:U^{4+}$, which is higher in energy than the $5f^{n-1}6d(t_{2g})^1$ manifold and lower than the $5f^{n-1}6d(e_g)^1$ manifold. The electronic structure of the $5f^1 7s^1$ states is found to be very different from that of the $5f^1 6d(t_{2g})^1$ ones. Whereas the latter can be considered impurity levels, the delocalized nature of the $5f^1 7s^1$ states indicates that they might be considered U^{4+} trapped excitons, using the terminology proposed by McClure and Pedrini.[33] Furthermore, some members of the $5f^{n-1}6d(e_g)^1$ set seem to be notably influenced by the $5f^1 7s^1$ states through a considerable interconfigurational mixing. All of this makes the electronic structure of the levels lying at high energies more complex than that of isomorphous and similar systems studied before (like $Cs_2ZrCl_6:Pa^{4+}$, $Cs_2NaYCl_6:U^{3+}$, and $Cs_2ZrCl_6:U^{4+}$, from Refs. 34, 21, and 28, respectively), where the $5f^1 7s^1$ set was not found at comparable energies. However, since the $5f^1 6d(t_{2g})^1$ manifold is lowest in energy and closest to the $5f^2$ manifold, the optical properties of the material should be primarily determined by the $5f^2 \leftrightarrow 5f^1 6d(t_{2g})^1$ electronic transitions. Consequently, in this work we concentrate on the study of the electronic structure of the $5f^1 6d(t_{2g})^1$ manifold and on the $5f^2 \to 5f^1 6d(t_{2g})^1$ absorption spectrum combining the results of the methods described in Sec. III with the experimental absorption spectrum obtained as described in Sec. II. Given the delocalized nature of the $5f^1 7s^1$ manifold, mentioned above, and its interaction with the higher $5f^{n-1}6d(e_g)^1$ states, spe-

TABLE II. Spectroscopic constants of the $5f^16d(t_{2g})^1$ manifold of Cs$_2$GeF$_6$:(UF$_6$)$^{2-}$. Spin-free Hamiltonian calculations. U–F bond distances, R_e (in Å), totally symmetric vibrational frequencies, $\bar{\nu}_{a_{1g}}$ (in cm^{-1}), and minimum-to-minimum energy differences, T_e (in cm^{-1}). Manifold averages and mean square deviations of the individual values with respect to the averages are labeled as $\langle 5f^16d(t_{2g})^1\rangle$.

State	CASSCF($5f,6d,7s$)			MS-CASPT2(F48,U20)		
	R_e	$\bar{\nu}_{a_{1g}}$	T_e	R_e	$\bar{\nu}_{a_{1g}}$	T_e
$\langle 5f^16d(t_{2g})^1\rangle$	2.181±0.005	587±4		2.154±0.007	568±6	
1 $^3T_{1u}$	2.171	590	36 474	2.143	559	36 222
1 $^3T_{2u}$	2.177	585	38 649	2.149	560	38 191
1 $^3A_{1u}$	2.177	583	42 533	2.150	568	39 413
2 $^3T_{1u}$	2.177	583	43 655	2.149	559	40 477
1 ^3E_u	2.178	581	41 802	2.152	565	41 007
1 $^3A_{2u}$	2.187	583	42 144	2.164	571	42 682
2 ^3E_u	2.185	585	46 772	2.165	570	45 493
3 $^3T_{1u}$	2.188	588	46 858	2.163	562	45 771
2 $^3T_{2u}$	2.189	585	47 701	2.163	562	46 256
1 $^1A_{1u}$	2.176	587	35 180	2.151	570	35 650
1 $^1T_{1u}$	2.181	591	39 430	2.148	572	37 663
1 ^1E_u	2.184	581	41 054	2.155	569	38 997
1 $^1T_{2u}$	2.182	589	44 594	2.149	566	42 839
2 $^1T_{1u}$	2.177	593	51 293	2.142	580	46 009
2 ^1E_u	2.185	589	50 026	2.160	573	46 540
2 $^1T_{2u}$	2.188	594	50 993	2.160	579	46 731
1 $^1A_{2u}$	2.183	583	49 354	2.159	566	48 779
3 $^1T_{1u}$	2.181	591	57 539	2.151	575	52 917

cific theoretical work is in progress in our laboratory to establish the methodological requirements for their accurate characterization.

We have obtained the U–F equilibrium distances, R_e, and totally symmetric harmonic vibrational frequencies, $\bar{\nu}_{a_{1g}}$, of the $5f^16d(t_{2g})^1$ states from the numerical potential energy surfaces as in Ref. 35. The minimum-to-minimum transition energies relative to the $5f^2$-A_{1g} ground state, T_e, which should be very close to zero-phonon transitions, have also been calculated. All the results presented in this work include embedding effects associated with the Cs$_2$GeF$_6$ host, as described in Sec. III. The results obtained without spin orbit are presented in Table II; they allow us to deduce the effects of dynamic electron correlation by comparison of CASSCF($5f,6d,7s$) (without dynamic correlation) with MS-CASPT2(F48,U20) (with dynamic correlation) results; those including dynamic correlation and spin-orbit effects appear in Table III. The analysis of the embedded cluster spin-orbit wave functions in terms of spin-orbit-free $iS\Gamma$ wave functions is also presented in Table III for $R(\text{U}-\text{F})=4.10$ a.u. $=2.17$ Å. The results of Table III are the most accurate results of those presented in this work and are the ones to be used in order to discuss the electronic structure and absorption spectrum of Cs$_2$GeF$_6$:U^{4+}.

The values of the equilibrium distance R_e and vibrational frequencies $\bar{\nu}_{a_{1g}}$ of all spin-orbit levels, presented in Table III, show that the $5f^16d(t_{2g})^1$ manifold is formed by a set of quite parallel potential energy surfaces. The averages of the individual R_e and $\bar{\nu}_{a_{1g}}$ values over the manifold appear also in Table III followed by the standard deviations of individual values with respect to the averages (analogous averages have been computed with the spin-orbit-free results and appear in

Table II). Whereas electron correlation shortens the bond lengths by some 0.027 Å and decreases the a_{1g} vibrational frequencies by some 19 cm^{-1} (as deduced from the results in Table II); spin-orbit effects are negligible: 0.001 Å and -2 cm^{-1}, respectively, (cf. Tables II and III), which indicates that structural calculations can be done at spin-orbit-free level, as long as embedding and dynamic electron correlation are included, as in the MS-CASPT2(U20,F48) calculations. Comparison of the average bond lengths of the $5f^2$ (2.174±0.005 Å, Ref. 6) and $5f^16d(t_{2g})^1$ (2.155±0.005 Å) manifolds reveals a shortening by 0.019 Å. This result agrees with what has been found in other lanthanide and actinide defects in hexafluoride, chloride, and bromide coordination in solids,[21,28,36,37] CH$_3$CN solution,[36] and gas phase,[36] and in eightfold coordination in fluorite.[38]

As to the energy levels, the effects of dynamic electron correlation that can be inferred from Table II are better understood if compared to the electron correlation effects calculated on isomorphous Cs$_2$ZrCl$_6$:U^{4+}.[28] In the latter, a general stabilization due to dynamic electron correlation was found ranging from 3300 to 8700 cm^{-1} that averages to 5500±1600 cm^{-1}. In the fluoride crystal, analogous stabilizations are also observed, but are smaller by about 3600±490 cm^{-1}. In effect, the electron correlation effects deduced from Table II range from +470 to -5300 cm^{-1} and average to $-1800±1800$ cm^{-1}. The fact that electron correlation effects are smaller in the fluoride than in the chloride can be seen as an expression of the less covalent character of the fluoride, compared to the chloride system. Also interesting is the comparison of the spin-orbit energy levels calculated in both crystals. The order of spin-orbit states found in our calculations and presented in Table III shows only a few

TABLE III. Results of *sfss* spin-orbit WB-AIMP $(UF_6)^{2-}$ embedded cluster calculations that include Cs_2GeF_6 embedding, 68 valence electron correlation, and relativistic effects, including spin-orbit coupling. U–F bond distances, R_e (in Å), totally symmetric vibrational frequencies, $\bar{\nu}_{a_{1g}}$ (in cm⁻¹), minimum-to-minimum energy differences, T_e (in cm⁻¹); oscillator strengths, f; and analysis of the spin-orbit wave functions of Cs_2GeF_6:$(UF_6)^{2-}$. Manifold averages and mean square deviations of the individual values with respect to the averages are labeled as $\langle 5f^1 6d(t_{2g})^1 \rangle$. For comparisons: R_e=2.165 Å for the ground state $5f^2 - 1A_{1g}$ (Ref. 6).

State	R_e	$\bar{\nu}_{a_{1g}}$	T_e	$f\times10^{2a}$	Weights of spin-orbit-free wave functions[b]							
$\langle 5f^1 6d(t_{2g})^1 \rangle$	2.155±0.005	566±8										
$1\,E_u$	2.147	559	38 519		73.87	$1\,^3T_{1u}$	20.41	$1\,^3T_{2u}$				
$1\,T_{2u}$	2.148	560	38 744		78.21	$1\,^3T_{1u}$						
$1\,A_{1u}$	2.153	567	40 156		77.83	$1\,^1A_{1u}$	10.94	$3\,^3T_{1u}$	10.09	$1\,^3T_{1u}$		
$1\,T_{1u}$	2.150	567	40 428	6.552	50.57	$1\,^1T_{1u}$	18.20	$1\,^3T_{2u}$	11.82	$2\,^3T_{1u}$		
$2\,E_u$	2.156	565	42 137		59.31	$1\,^1E_u$	18.00	$2\,^3T_{1u}$	11.18	$2\,^3T_{2u}$		
$2\,T_{2u}$	2.155	560	42 612		54.49	$1\,^3T_{2u}$	15.12	$1\,^3E_u$	11.16	$1\,^3A_{2u}$		
$2\,T_{1u}$	2.152	554	42 641	3.273	30.06	$1\,^3T_{2u}$	20.65	$1\,^3A_{1u}$	19.80	$2\,^3T_{1u}$	12.69	$1\,^3T_{1u}$
$1\,A_{2u}$	2.152	561	43 174		84.59	$1\,^3T_{2u}$						
$3\,T_{1u}$	2.150	571	43 989	0.720	56.94	$1\,^3T_{1u}$	15.20	$1\,^3E_u$				
$3\,T_{2u}$	2.156	562	44 400		44.08	$2\,^3T_{1u}$	27.56	$1\,^1T_{2u}$	17.25	$2\,^3E_u$		
$2\,A_{1u}$	2.146	560	46 202		63.72	$2\,^3T_{1u}$	18.94	$3\,^3T_{1u}$	16.81	$1\,^3T_{1u}$		
$4\,T_{1u}$	2.152	567	46 206	1.806	37.13	$1\,^3E_u$	22.94	$1\,^1T_{1u}$	14.54	$2\,^3T_{2u}$	13.94	$1\,^3A_{1u}$
$3\,E_u$	2.150	559	46 492		59.28	$1\,^3T_{2u}$	16.94	$1\,^3T_{1u}$				
$4\,T_{2u}$	2.152	564	47 632		35.63	$1\,^3E_u$	19.92	$1\,^3T_{2u}$	17.52	$1\,^3T_{1u}$	13.22	$1\,^1T_{2u}$
$4\,E_u$	2.154	561	48 647		70.29	$2\,^3T_{1u}$	18.98	$1\,^1E_u$				
$5\,T_{1u}$	2.152	562	48 693	0.321	32.88	$2\,^3T_{1u}$	31.11	$3\,^3T_{1u}$	18.31	$1\,^3A_{1u}$		
$3\,A_{1u}$	2.145	559	49 005		71.62	$1\,^3T_{1u}$	12.29	$2\,^3T_{1u}$	12.02	$1\,^1A_{1u}$		
$5\,T_{2u}$	2.157	564	49 173		34.71	$1\,^3A_{2u}$	21.46	$2\,^3T_{1u}$	16.22	$1\,^3E_u$	11.81	$1\,^1T_{2u}$
$6\,T_{1u}$	2.152	552	49 824	0.030	34.58	$1\,^3T_{2u}$	21.43	$1\,^3T_{1u}$	13.91	$1\,^1T_{1u}$		
$4\,A_{1u}$	2.165	578	50 119		65.46	$3\,^3T_{1u}$	22.92	$2\,^3T_{1u}$				
$7\,T_{1u}$	2.158	574	50 216	0.042	25.17	$2\,^3E_u$	19.81	$3\,^3T_{1u}$	19.78	$2\,^3T_{2u}$	15.55	$1\,^3A_{1u}$
$6\,T_{2u}$	2.157	572	51 897		27.52	$1\,^3A_{2u}$	19.30	$2\,^3T_{2u}$	15.18	$1\,^1T_{2u}$	12.43	$2\,^1T_{2u}$
$5\,E_u$	2.161	569	52 621		50.35	$2\,^1E_u$	30.63	$2\,^3T_{2u}$	10.57	$1\,^1E_u$		
$8\,T_{1u}$	2.156	565	52 782	0.045	28.73	$2\,^1T_{1u}$	23.96	$3\,^3T_{1u}$	18.84	$2\,^3T_{2u}$	10.77	$2\,^3T_{1u}$
$2\,A_{2u}$	2.161	567	53 036		42.54	$1\,^1A_{2u}$	41.74	$2\,^3T_{2u}$	14.81	$1\,^3T_{2u}$		
$7\,T_{2u}$	2.161	566	53 173		45.71	$2\,^3E_u$	32.72	$2\,^1T_{2u}$	12.25	$2\,^3T_{1u}$		
$8\,T_{2u}$	2.158	577	53 462		33.55	$3\,^3T_{1u}$	14.91	$2\,^1T_{2u}$	11.31	$2\,^2T_{2u}$	10.08	$2\,^3E_u$
$9\,T_{1u}$	2.160	555	53 578	0.036	51.27	$2\,^3E_u$	25.74	$2\,^3T_{2u}$	11.70	$3\,^3T_{1u}$		
$6\,E_u$	2.159	567	53 976		44.20	$2\,^3T_{2u}$	31.31	$2\,^1E_u$	15.93	$3\,^3T_{1u}$		
$10\,T_{1u}$	2.155	598	54 076	0.036	51.20	$2\,^1T_{1u}$	18.94	$1\,^3E_u$				
$7\,E_u$	2.159	565	55 895		70.49	$3\,^3T_{1u}$	12.20	$2\,^1E_u$				
$9\,T_{2u}$	2.159	567	55 917		58.76	$2\,^3T_{2u}$	15.33	$1\,^1T_{2u}$	10.22	$1\,^3E_u$		
$10\,T_{2u}$	2.161	565	57 707		47.37	$3\,^3T_{1u}$	27.61	$2\,^1T_{2u}$	18.78	$2\,^3E_u$		
$3\,A_{2u}$	2.159	563	59 195		51.14	$2\,^3T_{2u}$	48.70	$1\,^1A_{2u}$				
$11\,T_{1u}$	2.154	576	60 938	0.000	83.27	$3\,^3T_{1u}$						

[a] Oscillator strengths for the $1A_{1g}\rightarrow iT_{1u}$ absorptions were calculated at the ground state equilibrium distance: 2.165 Å.

[b] Weights are given in% and correspond to calculations at R(U–F)=2.17 Å. Only weights larger than 10% are given.

changes compared to that found in Cs_2ZrCl_6:U^{4+},[28] but the overall effect of the Cl to F chemical substitution is a large increase in energy ranging from 7300 to 10 100 cm⁻¹ that averages to 9100±650 cm⁻¹. These results in a solid phase are in qualitative agreement with what was observed by Ryan *et al.*[39] in octahedral hexafluoro and hexachloro complexes of U(IV) in solution, where they found shifts of about 8000 cm⁻¹ from the hexachloro to the hexafluoro complexes.

As a final remark on the electronic structure of the $5f^1 6d(t_{2g})^1$ manifold, it should be noted that the correlation between crystal levels and free ion levels is extremely uncertain in this system. This is a consequence of both crystal field and spin-orbit effects. The analyses presented in Table I point out a considerable mixing of free ion terms in the crystal. The mixing is also promoted by spin-orbit coupling, as ex-pressed by the analyses of the spin-orbit wave functions that are presented in Table III. As a result, it is very uncertain to assign free ion labels to the $5f^1 6d(t_{2g})^1$ levels and, therefore, this has not been done in Table III.

B. The $5f^2 \rightarrow 5f^1 6d(t_{2g})^1$ absorption spectrum of Cs_2GeF_6:U^{4+}

The experimental absorption spectrum of Cs_2GeF_6:U^{4+} single crystals, measured at 7 K between 190 and 350 nm, is presented in Fig. 1(a). It consists of a series of broad intense bands between 37 000 and 45 000 cm⁻¹ of which the first one, peaking at about 38 000 cm⁻¹, is the most intense. The spectrum shows no appreciable fine vibronic structure, so that detection of electronic origins is not possible.
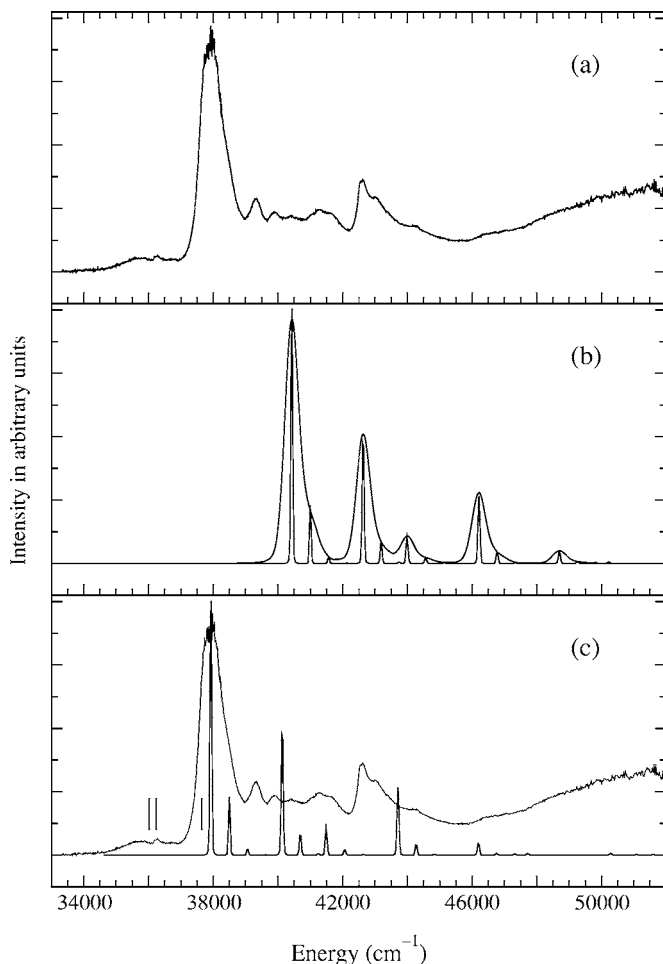
FIG. 1. $5f^2 \rightarrow 5f^16d(t_{2g})^1$ absorption spectrum of Cs$_2$GeF$_6$:U^{4+}. (a) Experimental spectrum, (b) theoretical spectrum obtained using relativistic AIMP embedded cluster results and different values for the line broadening parameter (100 and 5 cm^{-1} in the low and high resolution spectra, respectively), and (c) experimental spectrum and theoretical spectrum shifted by −2500 cm^{-1}. See text for details.

The absorption spectrum produced using the results of Table III can be observed in Fig. 1(b). We built the multiorigin absorption band profiles shown as follows. Firstly, we used the semiclassical time-dependent approach of Heller[40–42] to calculate the a_{1g} vibrational envelope of each individual electric dipole allowed transition $5f^2 - 1A_{1g} \rightarrow 5f^16d(t_{2g})^1 - iT_{1u}$ $(i=1,11)$. To do this, the equilibrium distance and a_{1g} vibrational frequency of the ground state $5f^2 - 1A_{1g}$ $(R_e=2.165$ Å, $\bar{\nu}_{a_{1g}}=564$ cm^{-1}, from Ref. 6) and of the $5f^16d(t_{2g})^1 - iT_{1u}$ excited states were used together with the corresponding minimum-to-minimum energy differences T_e (the values of R_e, $\bar{\nu}_{a_{1g}}$, and T_e for the iT_{1u} states appear in Table III). Secondly, we scaled the vibrational envelopes of the individual electronic origins so that their ratios coincide with the oscillator strength ratios; the oscillator strengths for the $1A_{1g} \rightarrow iT_{1u}$ transitions were calculated using the electric dipole transition moments between the $1A_{1g}$ and iT_{1u} spin-orbit wave functions and the Franck-Condon transition energies calculated at the ground state equilibrium distance, 2.165 Å; their values appear in Table III. Finally, we summed up all the individual, scaled progressions to obtain the final multiorigin a_{1g} band envelope. The formulas used to calculate the individual progressions allow for the use of an arbitrary line widening factor, Γ.[40–42] We used two different values: $\Gamma=5$ and $\Gamma=100$ cm^{-1}. The former allows to see the details of the progressions and leads to the absorption spectrum envelope of Fig. 1(b) that shows very narrow features; the latter was taken so as to make the width at half height of the first and most intense band to be similar to the experimental one; it leads to the absorption spectrum shown in Fig. 1(b) showing broader features. The narrow spectrum clearly shows the relative intensity of the members of each progression; in particular, it can be seen that the zero-phonon lines are the most intense in all cases, a characteristic that can be associated with the fact that the bond length change from the ground state to the excited states is small in this host and amounts −0.013 to −0.015 Å (see Table III). The comparison of the two spectra is useful since it shows how the less intense vibrational features contribute to the bands of the multiorigin a_{1g} envelope. Comparison of the experimental and calculated spectra shown in Figs. 1(a) and 1(b), respectively, suggests that the theoretical spectrum is high by about 2500 cm^{-1}. Consequently, the experimental spectrum is shown in Fig. 1(c), together with the theoretical one ($\Gamma=5$), after having shifted the latter by −2500 cm^{-1}. (Note that all spectra have been arbitrarily scaled so that the height of the first prominent and broad band coincides.)

Both the experimental and calculated band profiles agree in that the lowest band, peaking at about 38 000 cm^{-1}, is considerably more intense than the rest; this band can be safely assigned to the $5f^2 - 1A_{1g} \rightarrow 5f^16d(t_{2g})^1 - 1T_{1u}$ transition. Our calculations indicate that most of its intensity is due to the 0-0 transition and that it also includes the much less intense 0-1 and 0-2 members of the a_{1g} progression [Figs. 1(b) and 1(c)]. The $1T_{1u}$ origin is calculated to be at 40 428 cm^{-1}, which turns out to be some 2500 cm^{-1} too high compared to experiment; this discrepancy sets the error of the whole $5f^16d(t_{2g})^1$ manifold relative to the ground state. Part of this error can be related to atomic contributions. The corresponding $5f^2 - {}^3H_4 \rightarrow 5f^16d^1 - {}^3H_4$ transition is calculated 1000 cm^{-1} too high compared with experiments for the U^{4+} free ion when the same methods are used.[27]

The rest of the bands can be associated with the next four $5f^2 - 1A_{1g} \rightarrow 5f^16d(t_{2g})^1 - iT_{1u}$ $(i=2-5)$ electronic origins and their vibrational progressions. The calculations suggest that the second most intense band, observed in the experimental spectrum at about 42 600 cm^{-1}, can be associated with the fourth origin, $4T_{1u}$, and the features at 39 300, 41 200, and 44 200 cm^{-1}, with $2T_{1u}$, $3T_{1u}$, and $5T_{1u}$, respectively. However, in this region of the spectrum the agreement between the experimental and theoretical relative intensities is not so good. Whereas the $2T_{1u}$ origin is more intense than the $4T_{1u}$ one according to the calculations, the opposite trend is observed in the experimental spectrum. The comparison leads also to the conclusion that the calculated origins are more separated in energy than it can be deduced from the experimental spectrum. In effect, the $4T_{1u}-1T_{1u}$ energy difference is calculated to be about 5800 cm^{-1}, whereas the features assigned to the same levels are separated by roughly 4600 cm^{-1}, some 1000 cm^{-1} higher than the experimentally observed. Similar comparisons for the rest of origins allow to

roughly estimate the errors of the calculated origins within the $5f^16d(t_{2g})^1$ manifold as 900 ($2T_{1u}$), 400 ($3T_{1u}$), 1200 ($4T_{1u}$), and 2100 ($5T_{1u}$) cm^{-1}.

Finally, in Fig. 1(c) we have indicated, with vertical lines, the positions of the lowest $5f^16d(t_{2g})^1$ origins that are electric dipole forbidden in absorption: $1E_u$, $1T_{2u}$, and $1A_{1u}$. They appear shifted by -2500 cm^{-1} with respect to their calculated values (Table III), as the theoretical absorption spectrum. They indicate that the low intensity features observed in the 35 000 cm^{-1} region could be attributed to vibronic transitions to the close lying $1E_u$ and $1T_{2u}$. The lowest $1E_u$ level is found to be some 6200 cm^{-1} above the $5f^2$ level nearest in energy, which amounts some 11 vibrational quanta. This large energy gap could result in low nonradiative decay and efficient UV emission, which suggest the interest of investigating further this new material as a potential UV solid state laser.

V. CONCLUSIONS

Relativistic *ab initio* model potential (AIMP) embedded cluster calculations that include the quantum chemical effects of the Cs_2GeF_6 host, nondynamical and dynamical correlation of valence electrons (68, in this case), and relativistic effects, including spin-orbit coupling, have been done to compute the wave functions and energies of the $5f^16d(t_{2g})^1$ manifold of the octahedral $(UF_6)^{2-}$ defect clusters of the Cs_2GeF_6:U^{4+} material. The calculated totally symmetric vibrational frequencies of the ground $5f^2-1A_{1g}$ and $5f^16d(t_{2g})^1-iT_{1u}$ excited states ($i=1,11$), their energy differences, and their corresponding electric dipole transition moments have been used to compute the profile of the absorption spectrum as the superposition of the a_{1g} vibrational progressions of all electric dipole allowed $5f^2-1A_{1g} \rightarrow 5f^16d(t_{2g})^1-iT_{1u}$ transitions weighted by their respective calculated oscillator strengths. On the experimental side, single crystals of U^{4+}-doped Cs_2GeF_6 with 1% U^{4+} concentration have been grown by the Bridgman-Stockbarger method and their absorption spectrum has been measured at 7 K between 190 and 350 nm. The experimental spectrum shows a number of intense and broad absorption bands between 37 000 and 45 000 cm^{-1} of which the lowest, peaking at about 38 000 cm^{-1}, shows significantly more intensity than the rest; no appreciable fine vibronic structure is observed, so that, it is not possible to deduce the energy of the electronic origins from experiment only. Alternatively, the results of the quantum chemical calculations suggest that the experimental absorption spectrum can be assigned to $5f^2 \rightarrow 5f^16d(t_{2g})^1$ transitions and is due to the superposition of the vibronic structure built on the five lowest $5f^2-1A_{1g} \rightarrow 5f^16d(t_{2g})^1-iT_{1u}$ ($i=1-5$) electronic origins. Both the experimental and theoretical absorption spectrum profiles agree in that the first band, assigned to the $5f^2-1A_{1g} \rightarrow 5f^16d(t_{2g})^1-1T_{1u}$, is much more intense than the rest. The agreement is also good for the relative intensities of other three origins: $3T_{1u}$, $4T_{1u}$, and $5T_{1u}$, but it is comparatively poorer for the relative intensity of $2T_{1u}$. The five origins, responsible for the UV absorption spectrum observed, are calculated at 40 400, 42 600, 44 000, 46 200, and 48 700 cm^{-1}. The error of the calculated $5f^16d(t_{2g})^1$ manifold relative to the $5f^2$ ground state is 2500 cm^{-1}, as estimated in comparison with experiment.

[1] S. V. Godbole, A. G. Page, Sangeeta, S. C. Sabharwal, J. Y. Gesland, and M. D. Sastry, J. Lumin. **93**, 213 (2001).
[2] Sangeeta, S. C. Sabharwal, and J. Y. Gesland, J. Lumin. **93**, 167 (2001).
[3] N. Yu. Kirikova, M. Kirm, J. C. Krupa, V. N. Makhov, G. Zimmerer, and J. Y. Gesland, J. Lumin. **97**, 174 (2002).
[4] M. Kirm, J. C. Krupa, V. N. Makhov, E. Neodin, G. Zimmerer, and J. Y. Gesland, J. Lumin. **104**, 85 (2003).
[5] S. V. Godbole, A. C.-H. Lu, and A. G. Page, Radiat. Meas. **37**, 621 (2003).
[6] B. Ordejón, L. Seijo, and Z. Barandiarán, J. Chem. Phys. **123**, 204502 (2005).
[7] Z. Barandiarán and L. Seijo, J. Chem. Phys. **89**, 5739 (1988).
[8] L. Seijo and Z. Barandiarán, in *Computational Chemistry: Reviews of Current Trends*, edited by J. Leszczyński (World Scientific, Singapore, 1999), Vol. 4, p. 55.
[9] R. W. G. Wyckoff, *Crystal Structures* (Wiley, New York, 1968).
[10] L. H. Ahrens, Geochim. Cosmochim. Acta **2**, 155 (1952).
[11] R. D. Shannon and C. T. Prewitt, Acta Crystallogr., Sect. B: Struct. Crystallogr. Cryst. Chem. **25**, 925 (1969).
[12] L. Seijo, J. Chem. Phys. **102**, 8078 (1995).
[13] R. Llusar, M. Casarrubios, Z. Barandiarán, and L. Seijo, J. Chem. Phys. **105**, 5321 (1996).
[14] L. Seijo, Z. Barandiarán, and D. S. McClure, Int. J. Quantum Chem. **80**, 623 (2000).
[15] L. Seijo, Z. Barandiarán, and B. Ordejón, Mol. Phys. **101**, 73 (2003).
[16] Z. Barandiarán and L. Seijo, Can. J. Chem. **70**, 409 (1992).
[17] L. Seijo, Z. Barandiarán, and E. Harguindey, J. Chem. Phys. **114**, 118 (2001).
[18] T. H. Dunning and P. J. Hay, in *Modern Theoretical Chemistry*, edited by H. F. Schaefer III (Plenum, New York, 1977).
[19] J. Andzelm, M. Klobukowski, E. Radzio-Andzelm, Y. Sakai, and H. Tatewaki, *Gaussian Basis Sets for Molecular Calculations*, edited by S. Huzinaga (Elsevier, Amsterdam, 1984).
[20] B. O. Roos, P. R. Taylor, and P. E. M. Siegbahn, Chem. Phys. **48**, 157 (1980); P. E. M. Siegbahn, A. Heiberg, J. Almlöf, and B. O. Roos, J. Chem. Phys. **74**, 2384 (1981); P. Siegbahn, A. Heiberg, B. Roos, and B. Levy, Phys. Scr. **21**, 323 (1980).
[21] L. Seijo and Z. Barandiarán, J. Chem. Phys. **118**, 5335 (2003).
[22] K. Andersson, P.-Å. Malmqvist, B. O. Roos, A. J. Sadlej, and K. Wolinski, J. Phys. Chem. **94**, 5483 (1990).
[23] K. Andersson, P.-Å. Malmqvist, and B. O. Roos, J. Chem. Phys. **96**, 1218 (1992).
[24] J. Finley, P.-Å. Malmqvist, B. O. Roos, and L. Serrano-Andrés, Chem. Phys. Lett. **288**, 299 (1998).
[25] A. Zaitsevskii and J. P. Malrieu, Chem. Phys. Lett. **223**, 597 (1995).
[26] F. Rakowitz, M. Casarrubios, L. Seijo, and C. M. Marian, J. Chem. Phys. **108**, 7980 (1998).
[27] B. Ordejón, L. Seijo, Z. Barandiarán, and B. O. Roos (unpublished).
[28] Z. Barandiarán and L. Seijo, J. Chem. Phys. **118**, 7439 (2003).
[29] G. Karlström, R. Lindh, P. A Malmqvist *et al.*, Comput. Mater. Sci. **28**, 22 (2003).
[30] R. M. Pitzer, COLUMBUS suite of programs (ARGOS, CNVRT, SCFPQ, LSTRN, CGDBG, and CIDBG); See A. H. H. Chang and R. M. Pitzer, J. Am. Chem. Soc. **111**, 2500 (1989), and references therein for a description. L. Seijo, CNVRT and LSTRN have been adapted to handle AIMP integrals. M. Casarrubios, CIDBG has been modified for spin-free-state-shifted spin-orbit CI calculations.
[31] V. Vallet, L. Maron, C. Teichteil, and J.-P. Flament, J. Chem. Phys. **113**, 1391 (2000).
[32] Detailed core and embedding AIMP data libraries in electronic format are

available from the authors upon request or directly at the address http://www.uam.es/quimica/aimp/Data/AIMPLibs.html (see also Ref. 29).

[33] D. S. McClure and C. Pedrini, Phys. Rev. B **32**, 8465 (1985).

[34] L. Seijo and Z. Barandiarán, J. Chem. Phys. **115**, 5554 (2001).

[35] L. Seijo and Z. Barandiarán, J. Chem. Phys. **118**, 1921 (2003).

[36] Z. Barandiarán, N. M. Edelstein, B. Ordejón, F. Ruipérez, and L. Seijo, J. Solid State Chem. **178**, 464 (2005).

[37] F. Ruipérez, Z. Barandiarán, and L. Seijo, J. Chem. Phys. **123**, 204703 (2005).

[38] Z. Barandiarán and L. Seijo, Theor. Chem. Acc. (in press).

[39] J. L. Ryan, J. M. Cleveland, and G. H. Bryan, Inorg. Chem. **13**, 214 (1974).

[40] E. J. Heller, J. Chem. Phys. **62**, 1544 (1975).

[41] E. J. Heller, Acc. Chem. Res. **14**, 368 (1981).

[42] J. I. Zink and K. S. Shin, Adv. Photochem. **16**, 119 (1991).